# RESIDUAL GAS X-RAY BEAM POSITION MONITOR FOR PETRA-III

P. Ilinski*, BNL, Upton, NY 11973, U.S.A.

*Abstract*

The development effort is driven by the need for a new type of x-ray beam position monitor, which can detect the centre of gravity of the undulator beam. A residual gas x-ray beam position monitor for the PETRA III storage ring was developed and tested.

## INTRODUCTION

Blade type x-ray beam position monitors (XBMP) are currently employed at the third generation synchrotron facilities as "white" undulator beam XBPMs [1, 2]. They provide a micron accuracy resolution and are capable to withstand the high power of the undulator radiation. Nevertheless since the information of the beam position is obtained from the halo of the undulator radiation, the signal depends on the undulator gap and is affected by stray radiation from bending magnets and focusing optics. These can be overcome if XBPM will detect the centre of gravity of the undulator beam. XBPM based on the ionization of a residual gas can be considered a candidate for "centre of gravity white" beam position monitor.

## RESIDUAL GAS X-RAY BEAM POSITION MONITOR

Residual gas beam profile monitors were first developed to provide beam profile measurements at charged particles accelerators [3,4]. Development of residual gas x-ray beam position monitor (RGXBPM) for PETRA III undulator x-ray beams was performed at DESY [5]. The profile monitor consists of an ion chamber operated at a residual gas pressure in which ions or electrons are drifted in a parallel electrical field towards the micro channel plate (MCP), which amplifies the signal and produces an image of the beam profile on a phosphor screen, Figure 1.

### *Spatial Resolution*

The resolution of the residual gas beam profile monitors, which are in use at the particle accelerators is in the order of few hundreds of microns. Resolution of RGXBPM has to be substantially improved in order to comply with beam stability requirements at the third generation storage rings. Factors which define the RGXBPM resolution are: quality of the electrical field, initial kinetic energy of ions or electrons, resolution of detection system, and data processing. The electrical field has to be uniform in order to provide aberration free beam profile. Broadening of the beam profile occurs due to electrical field non-uniformity and presence of the transverse component of the electrical field. This broadening should not exceed the broadening of the beam profile, which is caused by the initial transverse kinetic energy of ions or electrons [6]. The resolution of detection system is defined by the MCP, the phosphor screen, optical coupling and signal to background ratio. A proper data processing allows sub-pixel resolution, where pixel characterizes the resolution of the detection system.

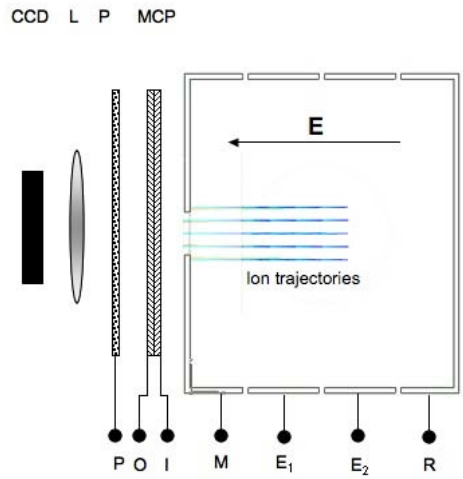


Figure 1: RGXBPM general layout: R - repeller electrode, $E_1$, $E_2$ - guide electrodes, M – mesh window electrode, I - MCP input, O - MCP output, P - phosphor screen, L - objective lens, CCD camera.

### *Signal Level*

The signal level of the RGXBPM first of all is defined by the total x-ray cross-section of the residual gas, which depends on gas pressure and composition. Typical pressure at the beamline can be better then $10^{-9}$ mbar, gas composition of UHV system is mostly hydrogen and may include nitrogen, water vapor etc.

In a typical ion chamber operating at gas pressure of about $10^{3}$ mbar a primary photoelectron will produce an avalanche of secondary electrons, so the number of created electron ion pairs will be proportional to deposited energy divided by average energy of one electron ion pair creation (35 eV for nitrogen). The upper level of residual gas pressure for RGXBPM is limited by presence of the MCP, and should not exceed $5x10^{-6}$ mbar. At such low pressure primary photoelectrons may not produce secondary electrons before been collected. Two scenarios are presented at Figure 2 for nitrogen and hydrogen at pressure of $10^{-6}$ mbar, and for detector length of 1 cm. First, when only primary photoelectrons are produced: (dotes) - nitrogen, (dash-dot-dot) - hydrogen, second for high gas pressure, when all secondary electrons were produced: (dashed) - nitrogen, (dash-dot) - hydrogen.

*pilinski@bnl.gov

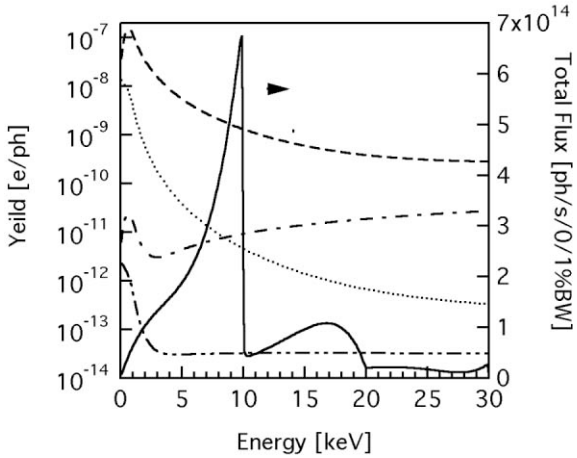


Figure 2: Electrons/ions yield at gas pressure of $10^{-6}$ mbar, 1-cm-collection-length; primary photoelectrons: (dotes) - nitrogen, (dash-dot-dot) - hydrogen; all secondary electrons: (dashed) - nitrogen, (dash-dot) - hydrogen.

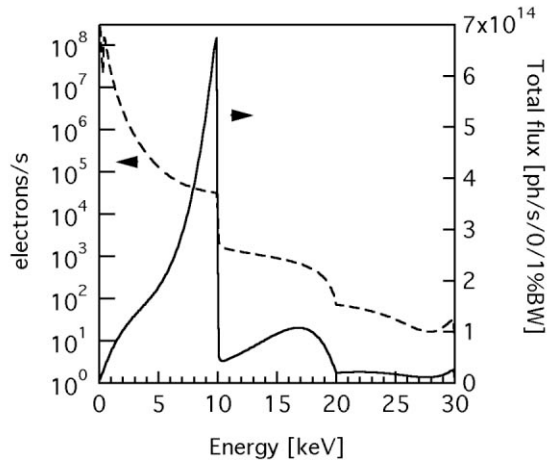


Figure 3: Current of primary photoelectrons, nitrogen gas, $10^{-6}$ mbar, 1-cm-collection-length; current generated by Total spectral flux of 2-m-long PETRA-III undulator, 2.9-cm-period-length, K = 0.6.

Photoelectron current, when only primary photoelectrons are produced, is presented at Figure 3 for 2-m-long PETRA-III undulator with 2.9 cm period length and for K = 0.6. As can be seen most of the photoelectrons are generated at low photon energies, even if the undulator radiation intensity at such energies is extremely low. Undulator radiation, which is "red shifted" from fundamental harmonic of undulator radiation, is radiated off-axis, which is illustrated at Figure 4 for the undulator flux distribution of 1 keV photons at 20 m for above undulator parameters. In case of low gas pressure the beam profile of integrated RGXBPM response is complicated. In case of high gas pressure, the signal is proportional to the deposited energy and observed beam profile will reflect power distribution of the undulator radiation, Figure 5.

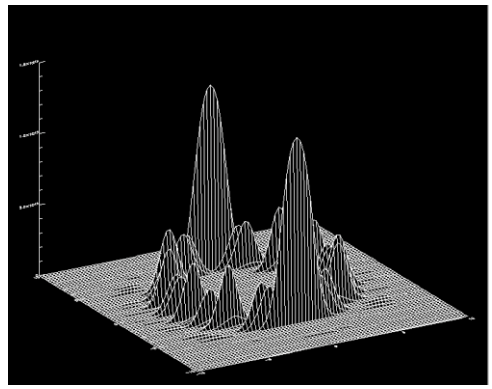

Figure 4: Flux density spatial distribution (20x20 $mm^2$) at 20 m of 1-keV-energy-photons, 2-m-long PETRA III undulator, 2.9-cm-period-length, K=0.6.

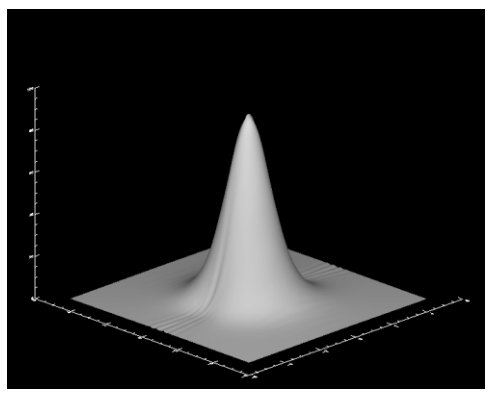

Figure 5: Undulator radiation power density distribution (10x10 $mm^2$) at 20 m, 2-m-long PETRA III undulator, 2.9-cm-period-length, K = 0.6.

## *General design*

Design specifications of RGXBPM for PETRA III have limitations for dimensions due to the fact that many of PETRA-III beamlines are equipped with canted undulators and separation of beamlines at RGXBPMs locations is small. Top view of RGXBPM design for canted undulator beamlines is shown in Figure 6. One RGXBPM assembly combines two RGXBPMs to monitor vertical and horizontal beam profiles. Internal active volume and electrodes of the RGXBPM have to be protected from any scattered or fluorescent x-ray radiation. For this purpose 5-mm-thick tungsten windows (W) are positioned in front and behind of each active volume and tungsten 100-mm-logn collimators are mounted in the front and at the exit of the RGXBPM assembly, Figure 7. Inner hole diameters are 17 and 18 mm for the upstream and downstream collimators, correspondingly. All electrodes of the RGXBPM are made of 1-mm-thick stainless steel with 1.5-mm-gaps between electrodes, which provides additional shielding of the RGXBPM active volume.

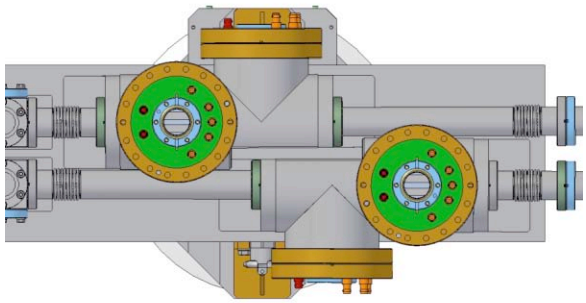

Figure 6: Top view of RGXBPM design for canted PETRA III undulator beamlines.

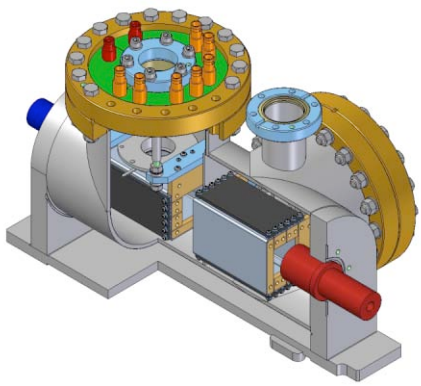

Figure 7: RGXBPM design includes vertical and horizontal monitors, upstream (red) and downstream collimators (blue).

The RGXBPM with an electrical readout equipped with Hamamatsu F3490-21S MCP with two split sow-tooth electrodes, which has effective area of 55 x 8 $mm^2$ and a channel diameter of 12 μm. For the RGXBPM with an optical readout a 32-mm effective diameter F2224-21P Hamamatsu MCP with a channel diameter of 10 μm and P43 phosphor screen is used. For tests a 50 mm focal length objective was used to image the beam profile from the phosphor screen onto a PCO PixelFly 12 bit CCD camera with 6.45-μm pixel size. The magnification of the optical system was chosen in order to have maximum field of view while not compromising the system special resolution, which was 15 μm/pixel.

## *Electrical Field Optimization*

Limited space dictated a compact RGXBPM design with small active volume, which makes optimization of the electrical field within the active volume extremely difficult. The CST Particle Studio™ software program was used for electrostatic modeling and to define ion and electron particle trajectories [7].

Geometry of electrodes and size of the active volume were optimized in order to achieve best field uniformity, minimize transverse field components and to provide maximum x-ray shielding of the active volume. The length, height and width of the active volume are 80x50x60 mm, Figure 8. In order to improve quality of the electrical field, the repeller electrode (R) and the mesh electrode (M) are bent at all edges, two 12-mm-wide guide electrodes (E1, E2) are placed in between the repeller and the mesh electrodes. Tungsten windows (W) are placed in front and behind active volume, they are also electrodes, which used to improve field quality at edges of the active volume.

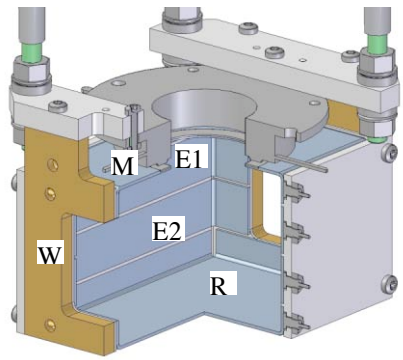


Figure 8: RGXBPM active volume.

Wiring of the RGXBPM is different for electrical and optical readouts, never the less optimal ratio of potentials was found to be the same: $(R\text{-}E_2)$:$(E_2\text{-}W)$:$(W\text{-}E_1)$:$(E_1\text{-}M)$ = 22:8:8:22. Symmetrical distribution of potentials is preferable, but this will require more HV power supply channels, Figure 9.

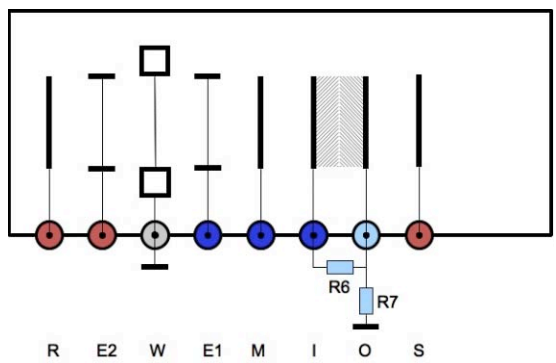


Figure 9: Symmetrical electrical wiring for optical readout, positive HV (red), negative HV (blue).

## *Test Results*

The RGXBPM performance was tested at the ESRF ID6 beamline, where it was installed in the front-end enclosure 30 m from the center of the straight section. Straight section included planar undulators with magnetic period length of 18 mm and 34 mm. A 300-μm-thick diamond window was located at 23 m. Horizontal mask of 2 mm was located at 14 m, vertical of 4 mm at 23 m. Horizontal and vertical slits were located at 26 m. Copper, 100-mm-long collimators, were installed before and after of the RGXBPM assembly in order to eliminate forward and back scattering radiation of striking electrodes. Upstream and downstream collimators were 8 and 10 mm diameters correspondingly. Slit sizes were fully opened to 4 mm vertically by 3.5 mm horizontally, which allowed most of the undulator radiation to pass through the RGXBPM.

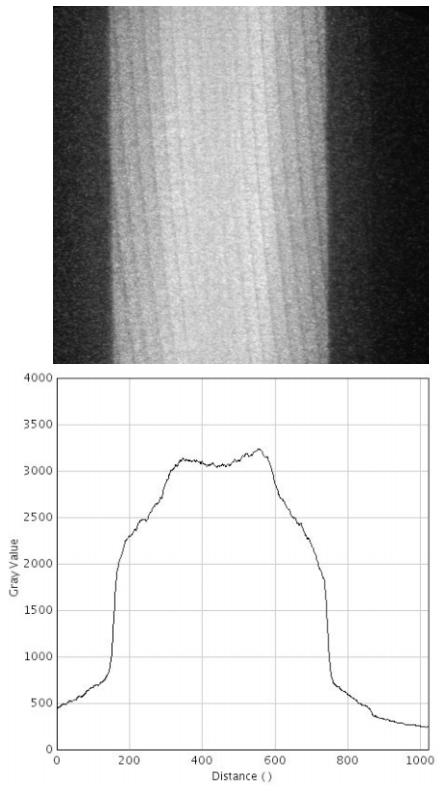


Figure 10: RGXBPM with optical readout. Image of the beam profile on the phosphor screen (top), ESRF undulator u18, 9-mm-gap, 500 ms exposure time; integrated cross-section of the beam profile (bottom).

Results of the RGXBPM test with optical readout are presented at Figure 10 for the ESRF undulator u18 at 9-mm-gap, first fundamental harmonic of undulator radiation was 16.7 keV. An image of the beam profile on the MCP phosphor screen is shown at the top picture, while the bottom is an integrated cross-section of the beam profile. Time of the CCD exposure was 500 ms. Centre of gravity was determined for each image of the beam profile, a time scan of centre of gravity is presented at Figure 11, as can be seen a 10 μm vertical translation of the RGXBPM can be clearly resolved. At the time of measurement, nitrogen gas pressure inside RGXBPM was controlled and set to be $4x10^{-6}$ mbar. For ions detection the repeller (R), guide (E2), (E1) and mesh (M) electrode potentials were set to 3800V, 1600V, 50V and -2200V, correspondingly. The MCP input (I) potential was set to -2200V, the MCP output (O) was grounded, and phosphor screen potential (S) was set to 4000V.

Integrated cross-section of the beam profile, Figure 10, has a minimum in the centre, which reflects a complex RGXBPM response of the undulator radiation, for which "red shifted" part is located off-axis, and where photoelectron yield cross-section is higher.

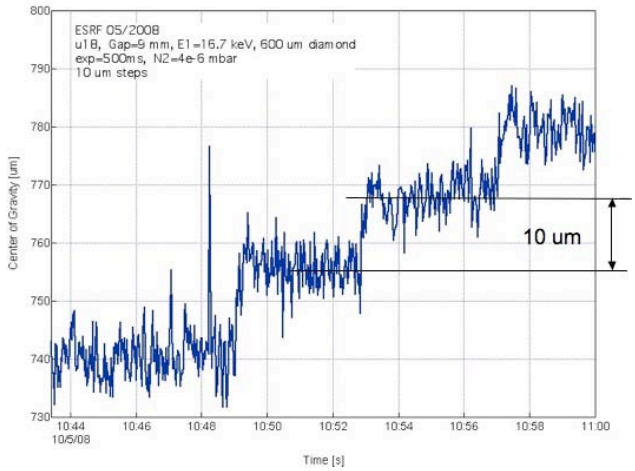


Figure 11: RGXBPM with optical readout. Time scan with 10 μm vertical translation steps of RGXBPM, u18, 9-mm-gap.

Test results of the RGXBPM with split sow-tooth electrode readout is presented at Figure 12, where time scan of signals from each electrode and normalized signal difference $(I_1-I_2)/(I_1+I_2)$ are shown for undulator u18 at gaps of 8, 10, 12 mm. For each gap entire RGXBPM assembly was scanned vertically with 20-μm-steps. At the time of measurement, the nitrogen gas pressure inside RGXBPM was $4x10^{-6}$ mbar, storage ring current 80 mA. For ions detection the repeller (R), guide (E1), (E2) and mesh (M) electrode potentials were set to 4650V, 2450V, 850V and -1500V, correspondingly. The MCP's input (I) and output (O) potentials were -1400V and -70V. Split electrodes were grounded through electrometers, signal level was 5 - 40 nA. As can be seen from Figure 13, where enlarged part of the scan from Figure 12 is shown, a 20 μm vertical translation of the RGXBPM is resolved.

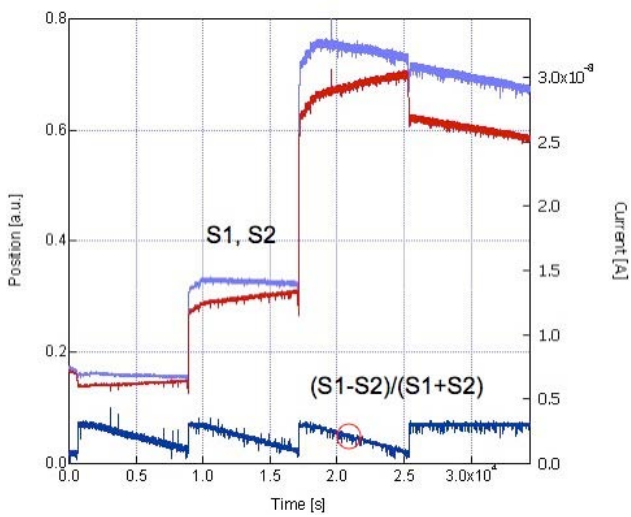


Figure 12: RGXBPM with electrical readout. Time scan with vertical translation steps of RGXBPM, u18, gaps of 8, 10, 12 mm.

Another way to test the RGXBPM was to observe controlled electron beam deflection, which occurred at the time of current injection. A time scans of normalized

signal difference $(I_1-I_2)/(I_1+I_2)$ of RGXBPM and electron beam angle deflection from e-bpms during injection are presented in Figure 14.

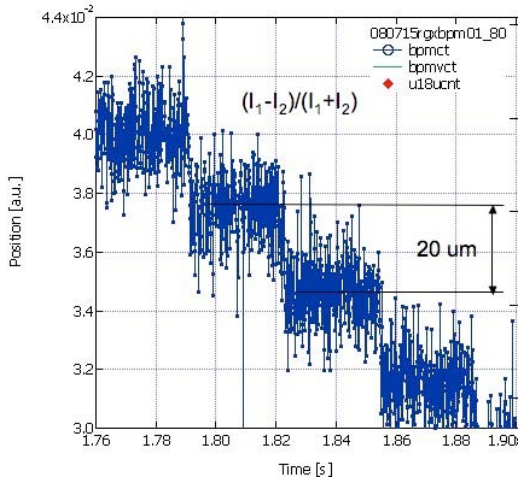


Figure 13: RGXBPM with electrical readout. Time scan with 20-μm vertical translation steps of RGXBPM, u18, 12-mm-gap.

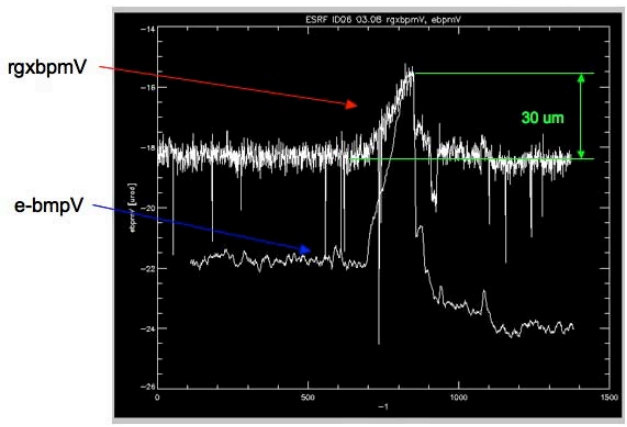


Figure 14: RGXBPM with optical readout. Time scan of beam position by RGXBPM and e-bpms during injection.

Operation of the RGXBPMs at PETRA III will be different form the results of tests at the ESRF ID06, since beamlines at PETRA III don't have fixed mask or windows. Spatial distribution of 1-keV energy photons at 20 m of PETRA III u29 with K=1.2 undulator radiation is shown in Figure 15 along with the footprint of ESRF ID06 mask. As can be seen 1-keV energy photons, which generate most of photoelectrons, will be recorded in case of PETRA III.

## CONCLUSIONS

Residual gas XPBM may be sensitive to jumps of gas pressure, MCP gain non-uniformity, and instability of the HV power supplies. In case if the beam is non-symmetrical, pressure changes may be interpreted as a beam position variation. Further studies of RGXBPMs have to be performed in order to ensure its reliable operation.

RGXBPMs may be effective monitors for undulators with complex radiation distribution, such as elliptical undulators, and for soft x-ray insertion devices, for which photo ionization cross-section in residual gas is substantial.

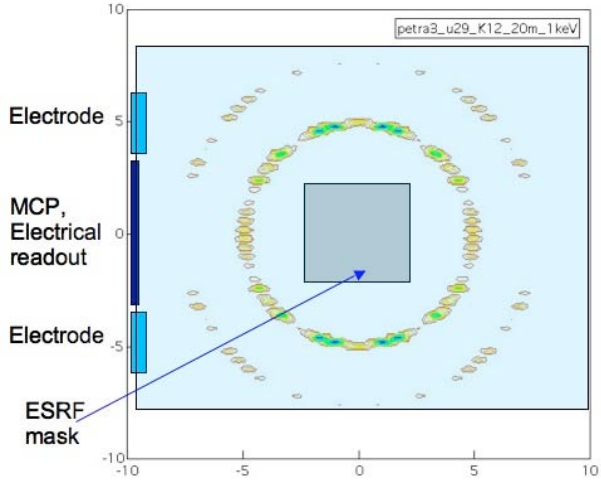


Figure 15: Spatial distribution of 1-keV energy photons at 20 m of PETRA III undulator u29, K=1.2.

## AKNOWLEDGMENTS

Development of the RGXBPM was conducted at DESY with support of U. Hahn, H. Schulte-Schrepping, S. Mueller, N. von Bargen, M. Degenhardt, and T. Korsch. The authors also would like to acknowledge J.-C. Biasci, C. Detlefs, H.-C. Wille and T. Roth for their help in RGXBPM tests at the ESRF.

## REFERENCES

1. O. Singh and G. Decker, "Operational Experience with X-ray Beam Position Monitors at the Advanced Photon Source", Proc. PAC 2001, Chicago, USA, 2001, IEEE 0-7803-7191-7/01, pp 539-543.
2. J. Krempasky, M. Böge, T. Schilcher, V. Schlott, T. Schmidt, "The use of Photon Monitors at the Swiss Light Source", Proc. EPAC 2004, Lucerne, Switzerland, 2004, pp 2520-2522.
3. F. Hornsta, W. H. Deluca, "Nondestructive beam profile System for the Zero Gradient Synchrotron", Proc. Six International Conference on High Energy Accelerators, M. I. I., Cambridge, MA, 1967, p. 374.
4. G. I. Budker, G. I. Dimov, V. G. Dudnikov, *Sov. At. Energy*, **22**, 441 (1967).
5. P. Ilinski, U. Hahn, H. Schulte-Schrepping, M. Degenhardt "Residual Gas X-ray Beam Position Monitor Development for PETRA III", AIP Conf. Proc. **879**, 782, (2007).
6. W. H. Deluca, "Beam Detection using Residual Gas Ionization", *IEEE NS*, **16**, 813- 822 (1969).
7. CST Particle Studio™, **CST GmbH**, Bad Nauheimer Str. 19, Darmstadt, Germany.